ChemistryOpen

Full Papers
doi.org/10.1002/open.202100153

Chemistry Europe
European Chemical Societies Publishing

www.chemistryopen.org

Experimental and Theoretical Study of the Ultrafast Dynamics of a Ni$_2$Dy$_2$-Compound in DMF After UV/Vis Photoexcitation

S. Sold,[a] B. C. Mummaneni,[a] N. C. Michenfelder,[b] Y. Peng,[c, d] A. K. Powell,[c, d] A.-N. Unterreiner,[b] G. Lefkidis,*[a, e] and W. Hübner[a]

We present a combined experimental and theoretical study of the ultrafast transient absorption spectroscopy results of a {Ni$_2$Dy$_2$}-compound in DMF, which can be considered as a prototypic molecule for single molecule magnets. We apply state-of-the-art *ab initio* quantum chemistry to quantitatively describe the optical properties of an inorganic complex system comprising ten atoms to form the chromophoric unit, which is further stabilized by surrounding ligands. Two different basis sets are used for the calculations to specifically identify two dominant peaks in the ground state. Furthermore, we theoretically propagate the compound's correlated many-body wave-function under the influence of a laser pulse as well as relaxation processes and compare against the time-resolved absorption spectra. The experimental data can be described with a time constant of several hundreds of femtoseconds attributed to vibrational relaxation and trapping into states localized within the band gap. A second time constant is ascribed to the excited state while trap states show lifetimes on a longer timescale. The theoretical propagation is performed with the density-matrix formalism and the Lindblad super-operator, which couples the system to a thermal bath, allowing us to extract relaxation times from first principles.

1. Introduction

The idea of mixing 3*d* and 4*f* metal ions within molecular systems has recently received increasing attention especially in the field of single molecule magnets (SMMs). Here the cooperativity amongst the paramagnetic metal ions is often difficult to unravel. The exchange coupling is expected to be relatively small, but the dipolar coupling should be significant,

especially in cases where strongly anisotropic 4*f* Ising ions such as Dy(III) are present. One of the most intriguing aspects here is the fact that in some cases the presence of 3*d* ions has a moderating effect on the usually very fast relaxation processes of 4*f* metal ions like Dy(III).[1] Indeed, it has been shown that the usual "shortcuts" through the energy barrier to spin reversal for the 4*f* components can be quenched by providing a suitable 3*d* metal ion - in the best cases so far identified this is the Co(II) ion in its high spin configuration.[1,2] On examining single ion properties in terms of magnetization relaxation processes it is clear that in addition to theoretical approaches an appropriate experimental method is to use very fast UV/Vis pump-probe femtosecond spectroscopy to help unravel details of the electronic state rearrangements.[3] We can note here that the single ion relaxation processes of 4*f* ions are regularly within a timescale of 10^{-10} to 10^{-15} seconds, which makes ultrafast techniques such as femtosecond spectroscopy extremely relevant. Given that it is always desirable to probe electronic structures using a multitechnique approach, preferably with experimentation as well as theory, we decided to investigate a Ni$_2$Ln$_2$ system which has the benefit of being accessible to theory as well as further experimentation. The magnetic details in terms of susceptibility, slow relaxation of the magnetization and spin state of the system have already been published and here we expand on these results by closely examining the possibility that vibrational modes contribute to the zero-field tunneling observed in the microSQUID measurements on oriented single crystal arrays.[4] We use theory and femtosecond spectroscopy to aid in gaining further insights into this system. This study provides a useful approach and way forward for examining the effect of processes operating on various time-

[a] S. Sold, B. C. Mummaneni, G. Lefkidis, W. Hübner
Department of Physics and Research Center OPTIMAS,
Technische Universität Kaiserslautern,
P.O. Box 3049, 67653 Kaiserslautern, Germany
E-mail: lefkidis@physik.uni-kl.de
[b] N. C. Michenfelder, A.-N. Unterreiner
Institute of Physical Chemistry,
Karlsruhe Institute of Technology,
Fritz-Haber-Weg 2, 76131
Karlsruhe, Germany
[c] Y. Peng, A. K. Powell
Institute of Inorganic Chemistry,
Karlsruhe Institute of Technology,
Engesserstrasse 15, 76131
Karlsruhe, Germany
[d] Y. Peng, A. K. Powell
Institute of Nanotechnology,
Karlsruhe Institute of Technology,
Hermann-von-Helmholtz-Platz 1,
76344 Eggenstein-Leopoldshafen, Germany
[e] G. Lefkidis
School of Mechanics,
Civil Engineering and Architecture,
Northwestern Polytechnical University,
Xi'an 710072, China

scales which shed light on relaxation pathways in such molecular-based SMM systems.

"Single Molecule Magnets" are called like this in the first place, because they act like a bulk material even though they are molecules. The best analogy is perhaps with superparamagnetic magnetic nanoparticles.[5–7] The [Dy$_2$Ni$_2$(L)$_4$(NO$_3$)$_2$(DMF)$_2$] structure investigated in this manuscript (Figure 1) has already been successfully synthesized and characterized.[8] This relatively small molecule, which contains two Ni and two Dy atoms, can act as a prototypic system for coordination clusters of transition metals covalently bound to oxygen, in which the magnetic and optical properties can be fine-tuned by adjacent lanthanides.[9–11] Nonetheless, its size still allows relatively accurate and reliable theoretical calculations by specifically addressing the various electronic excited states.

The "butterfly" structure of the ligand is a defect-dicubane core topology coordination. Especially for tetranuclear 3d-4f clusters, this is one of the more familiar structural motifs in magneto-chemistry.[12] The Schiff-based ligand ((E)-2-(2-hydroxy-3-methoxybenzylideneamino)phenol, (H$_2$L) has two types of pockets:[13] Pocket-I, ONO-donating; Pocket-II, OO-donating. Dy$_2$Ni$_2$ was synthesized as described by Mondal *et al.*[8] and dissolved in dimethylformamide for steady state and transient absorption experiments.

Interestingly, it has been found before that defect-dicubane compounds exhibit single molecular magnet behavior with significant barriers to spin reorientation.[14–16] A similar behavior was also observed in several 3d–4f coordination clusters with different core topologies.[17–31]

Transient absorption has been employed for decades in order to measure time-dependent optical phenomena on various time scales. Especially on the ultrafast (subpicosecond) time scale it represents an important investigation tool, e.g., for the energy transfer in a photosynthetic membrane, which typically takes place on a time scale of less than 100 fs.[32] In general the technique involves two laser pulses, i.e., a pump and a probe laser pulse which jointly interact with a sample. The pump pulse produces a nonlinear optical response in the sample and influences the absorption of the probe pulse, leading to a stroboscopic detection of the absorption properties of the sample. Quite often, as in our work, the detected absorption spectra are put in relation to the ground state spectrum and consequently the difference spectra are given. Although generally these excitation processes are well understood,[33,34] the exact molecular orbitals participating in the virtual excitations of the pertinent many-body states are often challenging to identify and analyze.

Mostly the investigated samples are not disconnected from the environment.[35] In order to give a theoretical explanation of the experimental physics a description of the sample as a closed quantum system is insufficient. In this contribution the density matrix formalism is used for the theoretical calculations. The Lindblad superoperator describes the interaction of the sample with its environment leading to energy dissipation, decoherence and relaxation effects.[36]

Interesting physics has been found in magnetic materials on similar time scales, i.e. picoseconds (ps) 10^{-12} s and femtoseconds (fs) 10^{-15} s. The milestone experiment of Beaurepaire *et al.* in 1996,[37] which for the first time showed laser-induced demagnetization in ferromagnetic Ni in the subpicosecond regime was the starting point of a quickly growing field and attracted great interest,[38–43] since it showed how to manipulate
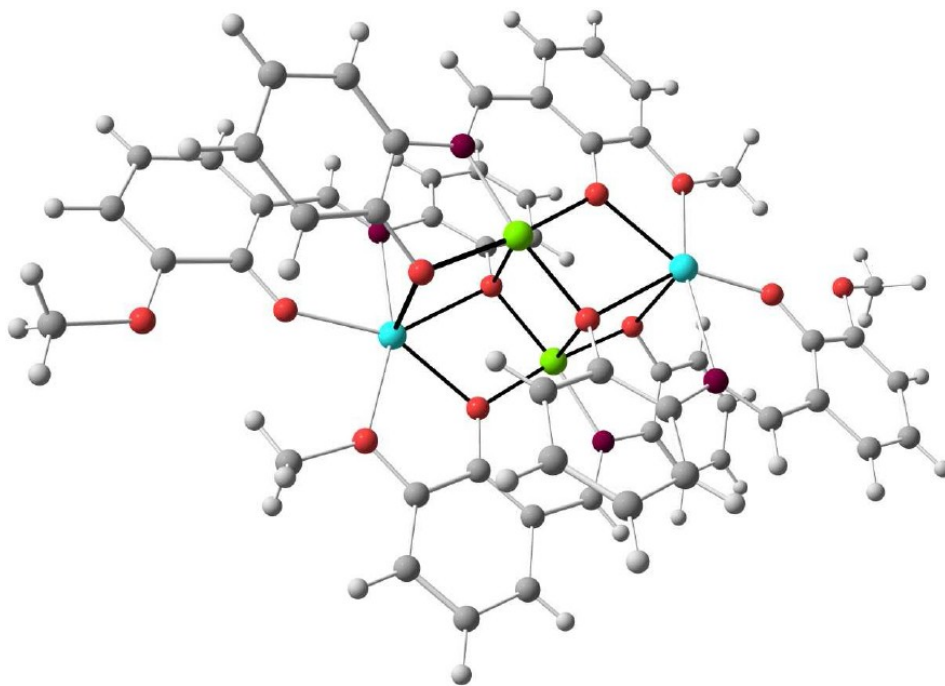
Figure 1. The complete {Dy$_2$Ni$_2$} complex. The {Dy–O–Ni} core is emphasized with the darker bonds. The molecule has no charge. (Dy: cyan, Ni: green, O: red, N: magenta, C: dark gray, H: light gray).

the spin state of magnetic materials orders of magnitude faster than before and thus opened the way to "spintronics" applications (i.e., logic devices in which the spin rather than the charge of the electrons take over the role of the information carrier).[44–48] This promising perspective among others also launched investigation of many different functionalities based on Λ processes (i.e., electronic excitation of a system to an intermediate state immediately followed by a deexcitation to a different state than the original one, all with a single laser pulse) and the applicability on real, synthesized structures.[35,49–51] Furthermore, also more complicated processes, such as the V and the four-photon M processes (the letters Λ, V, and M roughly indicate the energy positions of the involved electronic states), also in conjunction with bath reservoirs, have been investigated.[52,53] Note that slow direct relaxation is a prerequisite for the success of the coherent Λ, V, and M processes, corroborating the joint role of f and d electrons in these types of systems. Element-resolved laser-induced magnetization dynamics was also reported in $3d$-$4f$ systems, such as the ferrimagnetic CoDy.[54]

Since the Ni_2Dy_2-system or any other related system do not show luminescence, it is expected that there are other dominating relaxation channels after photoexcitation, which occur on an ultrafast timescale (ps and fs). One commonly used method to explore this time scale is transient broadband absorption spectroscopy. Typically, the analysis is straightforward as it can be analysed linearly after some coherent artefacts around time zero. Often, the analysis does not require sophisticated calculations of nonlinear coupling terms and can, in principle, be directly compared with theoretical calculations of excited states. Finally, the excitation intensities applied in transient absorption spectroscopy can be kept comparably moderate resulting in higher photo stability of this group of complexes.

For the theoretical description of our highly correlated magnetic system we employ an adequate post-Hartree-Fock quantum-chemistry method, from the coupled-cluster family. Generally coupled-cluster methods are capable of adequately describing both static correlations (which dominate magnetism) and dynamical correlations (which govern the optical properties, since they consist of charge-transfer virtual excitations).[55] At the same time, being size-consistent it allows for much better description of geometry deformations (such as vibrations) than the simpler configuration-interaction based methods for both the ground and the electronically excited states.[56–58]

In our joint experimental and theoretical study we mainly investigate the dynamics of the cluster after the excitation with a laser pulse, and compare the observed ultrafast transient absorption spectra with state-of-the-art quantum chemistry. Our approach allows us to not only compare the experimental and the theoretical relaxation times, but to also assign the specific electronic transitions involved (at least on a semi-quantitative basis), as well as to analyze their charge-transfer nature.

2. Static Properties

Before we delve into the investigation of the dynamic properties of the system, which is our main goal, we must first perform some static quantum chemical calculations and compare their results with experimental spectra, in order to assess their validity. Furthermore, the analysis of the energy levels, can give us some additional insight into the microscopic mechanisms involved in the dynamics studied in the next section.

2.1. Energy Levels

For our *ab initio* calculations we employ the high-level coupled-cluster method with single and double excitations (CCSD),[59–61] followed by the the equation-of-motion CCSD (EOM-CCSD) for the excited states,[58,62] as implemented in the GAMESS quantum chemistry package,[63] and the perturbative inclusion of spin-orbit coupling (SOC) and a static magnetic field (Zeeman splitting, to distinguish between spin-up and spin-down states). In our experience, this combination is a very good compromise between incorporating enough static correlations to adequately describe most of the $d-d$ transition states (missing only few of the higher multiplicity states), which govern magnetism, and the satisfactory description of the charge-transfer states, which are responsible for the optical excitations. For the non-metallic atoms we use Slater-type basis sets: STO-2G for the hydrogens and STO-6G for the rest.[64] For the two Ni atoms we use the SPK-DZC basis set,[65] while for the two Dy atoms we use and compare two different basis sets, i.e., SARC-ZORA[66] and WTBS.[67,68] The resulting many-body energy level scheme is shown in Figure 2. Although after the inclusion of SOC the spin $\hat{S}^2$ is not a good quantum number anymore, inspection of the ground-state wavefunction reveals that the ground state can be approximately considered a triplet state. In the remainder of
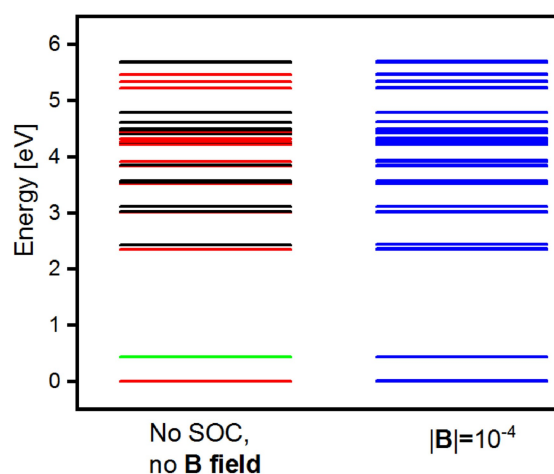
Figure 2. Level schemes of the $\{Dy_2Ni_2\}$ complex without (left) and with (right) SOC and a magnetic field, calculated with the SARC-ZORA and the SPK-DZC basis set for Dy and the Ni, respectively. Green is the reference (CCSD) state. Red are the triplet states, and black the singlet states. Blue are the states after the inclusion of SOC, for which $\hat{S}^2$ (and hence the multiplicity) is not a good quantum number anymore.

ChemistryOpen

Full Papers
doi.org/10.1002/open.202100153

Chemistry Europe
European Chemical
Societies Publishing

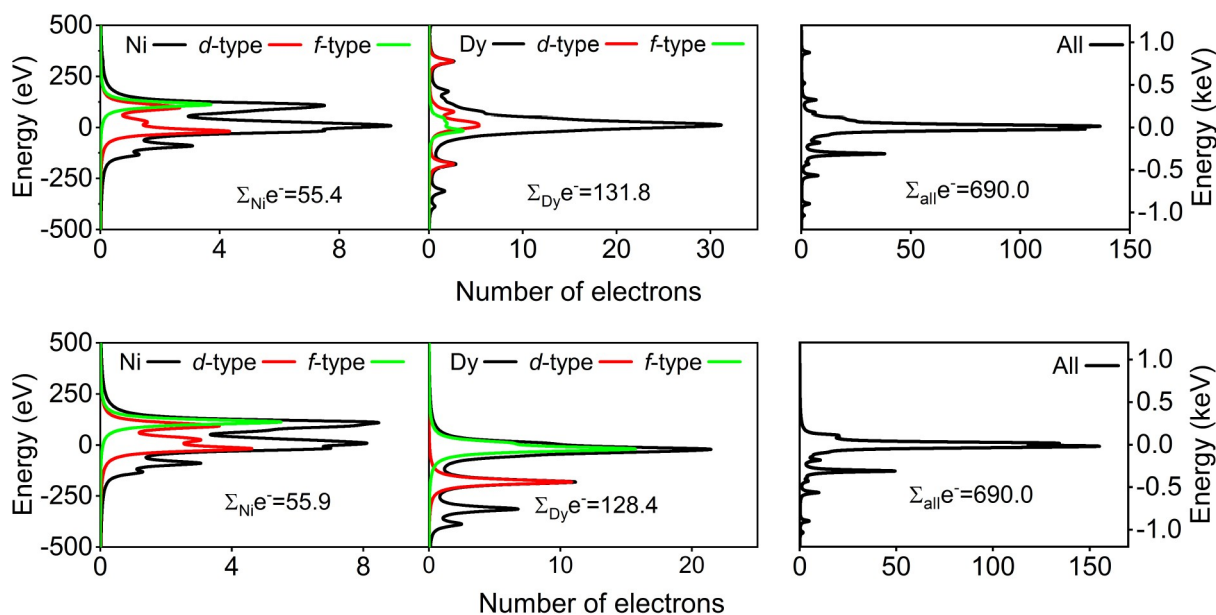this manuscript the words "singlet" and "triplet" should be understood in a similar loose manner.

The importance of the static correlations is revealed if one looks at the main virtual transition of the ground state, namely from the highest occupied molecular orbital (HOMO) to the lowest unoccupied molecular orbital (LUMO), for both basis sets (Figure 3), amounting to a correlation energy of the order of 14 eV for the reference CCSD state (17 ppm of the total CCSD energy). For both basis sets, the HOMO and LUMO are mainly linear combinations of orbitals located on the Ni atoms (differing in the sign of their linear combinations) with a strong d character. The same strong static correlations are also found for higher many-body electronic states. Very interesting for our dynamics is the fact that there is a substantial difference in the participation of the metallic d atomic orbitals between molecular orbitals 341/342 and 345, which corresponds to a (partial) metal-oxygen charge transfer when exciting the compound with our laser pulses.

Due to the huge number of molecular orbitals, and in order to better understand the physics behind the correlation energy we also analyze the density of states and the partial density of states of the molecular orbitals at the Hartree-Fock level (Figure 4). Note that although the energies of the one-electron molecular orbitals do not correspond to the excitation energies

of our many-body wavefunctions, their analysis gives some insight into the distribution of the electron charges in the compound. One should bear in mind, however, that any charge analysis (e.g., Mulliken or Löwdin analyses) is based on the lossy projection of the one-electron density matrix out of a correlated, multiconfigurational wavefunction, accompanied by the arbitrary division of the overlap electronic population each among pairs of atoms to the participating atoms (e.g., equal division for the Mulliken analysis, or proportional to their electronegativities for the Löwding analysis). Therefore, although the charges often constitute a helpful qualitative tool, they can substantially differ from the formal charges expected from stoichiometry chemistry. Most of the one-electron (i.e., uncorrelated) states around the Fermi level are either d-character Ni orbitals or f-character Dy orbitals. The latter however, contribute with much lower amplitudes to the correlated ground and lower-lying many-body states. Thus, in total the correlation energy mainly stems from the static correlations of the d electrons of the Ni. From a more physical point of view, this also means that altering the local geometry of the Ni atoms (which in turn changes their respective ligand-field splitting) will have a dramatic impact on the energy level of the whole compound and thus change its dynamical behavior. More specifically, further lifting the degeneracies of

MO 341

MO 342

MO 345
(HOMO)

MO 346
(LUMO)
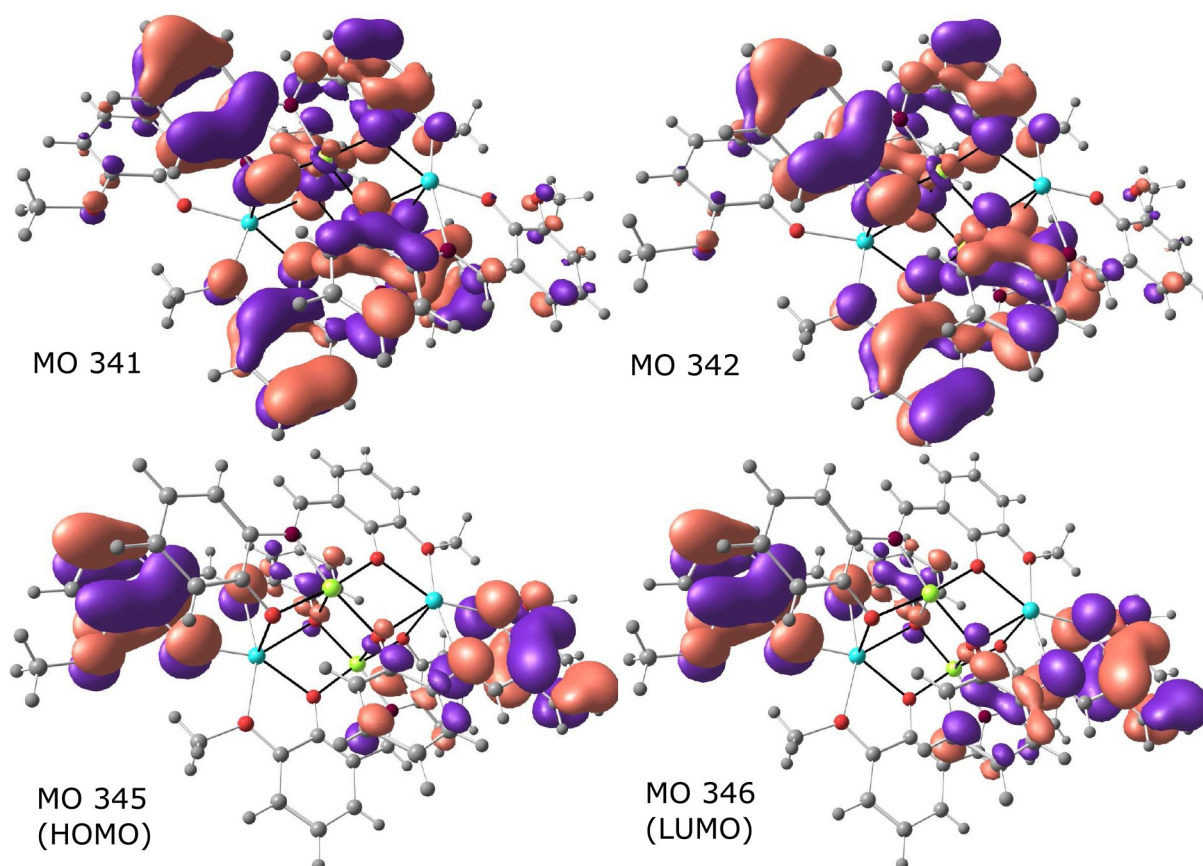
Figure 3. Some of the molecular orbitals participating in the virtual excitations of the ground and the excited manybody triplet states at about 3 eV (345→346 and 341/342→346), calculated with the SARC-ZORA basis set. The difference in the participation of the metallic d orbitals between molecular orbitals 341/342 and 345 corresponds to a (partial) metal-oxygen charge transfer when exciting the compound with our laser pulses. The virtual transition 341/342→346 is also the main contribution to the trap state $|11\rangle$ at 2.3 eV (see text).

ChemistryOpen

Full Papers
doi.org/10.1002/open.202100153

Chemistry
Europe
European Chemical
Societies Publishing

Figure 4. The density of states of the Ni (left), the Dy (middle) and the whole {Dy$_2$Ni$_2$} complex (right) with the SARC-ZORA (upper panel) and the WTBS (lower panel) basis set at the Hartree-Fock level. The black, the red and the green curves refer to the total, the d and the f density of states of each atom, respectively. The summation of all electronic density belonging to each category is also given.

the *d* orbitals will increase the excited state energies and decrease the exchange coupling between the four magnetic atoms.

The charge and the spin distribution is more or less similar for all many-body states of the coupled cluster calculations with SARC-ZORA. We find a $\approx +1.6$ charge on the ligands (distributed over all the non-metallic atoms), $\approx +0.5$ on the two Ni atoms, and almost 0 on the two Dy atoms. The spin is completely localized on the ligands. For WTBS the spin localization is similar. The charge distribution is very different, though. We find a positive charge density on the two Dy atoms (≈ 3.2) and a negative charge density on the ligands (≈ -1.5). There is no charge density on the Ni atoms.

2.2. Electronic Spectrum

As a first measure of trustworthiness of our quantum chemical calculations, in Figure 5 we compare the theoretical ground state spectrum (at temperatures $T = 0$ K and $T = 300$ K) with the experimentally measured one [the absorption spectra in a wavelength range between 200 and 800 nm were obtained with an UV/Vis/NIR spectrometer Cary 500 (Varian)].

For both basis sets the theoretical spectrum exhibits two peaks. For the coupled cluster calculation with the SARC-ZORA basis set the peaks are shifted to higher energies; weakly for the 305 nm and strongly for 415 nm. In case of WTBS basis set the shifting to shorter wavelength is a bit stronger for the 305 nm peak and much less for the 415 nm peak. The units on the *y*-axis are in at. un. In fact few dipole allowed transitions are found for the system calculated with SARC-ZORA and even fewer for WTBS. In the experimental spectrum we see two peaks and at least one shoulder. Again, one at a wavelength of
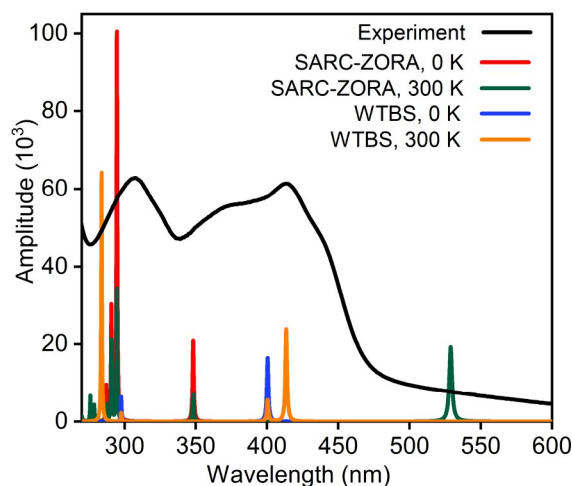
Figure 5. Experimental (in DMF as solvent) and theoretical (without solvent) ground state absorption spectra. The theoretical spectra were calculated with the SARC-ZORA and the WTBS basis sets and at two different temperatures (0 and 300 K). The peaks at around 400 nm (partially) correspond to charge-transfer excitations within the {Dy–O–Ni} core (cf. Figure 3).

305 nm, the other one at 415 nm. The broadening of the low energy peak towards shorter wavelength could stem from either another electronic transition (shoulder) or a vibrational progression due to the aromatic ring of the ligand. The coupled-cluster calculated spectrum with WTBS is in very good agreement with the experimental data, although it does not fully cover the low-energy tail (i.e., wavelengths being larger than 500 nm), where the SARC-ZORA calculation (at 300 K) adds an important peak.

ChemistryOpen

Full Papers
doi.org/10.1002/open.202100153

Chemistry Europe
European Chemical
Societies Publishing

2.3. Infrared Spectrum

Here we present the theoretically calculated vibrational spectrum of the system and compare with the experimental results. The theoretical spectrum is first obtained at the HF level, for which it is possible to calculate analytical derivatives of the total energy with respect to the atomic dislocations (Figure 6).

After analytically obtaining the normal modes, we use them to numerically calculate the vibration frequencies at the CCSD level of three modes in three different regions, namely in the intermetallic-vibration region (517 cm^{-1}), the mid-range region (1050 cm^{-1}), and at a higher range (3699 cm^{-1}). The single-point energy data thus obtained are fitted to both a quadratic and a cubic polynomial.[69] In fact both polynomials give results which can differ quite a lot from the analytic ones (some exemplary normal modes are given in Table 1). This, of course, is a result of the strong correlations in the system, which strongly depend on the exact interatomic distances (notably the static correlations). For example, mode 331, which mainly includes vibrations of two carbon atoms from a benzene ring (no static correlations there), does not differ significantly in the two calculations. Mode 101 on the other hand heavily involves an oxygen atom which bridges a Dy and a Ni metal, and thus is affected by the correlational level of the computational method. Correlations can generally both increase (e.g., mode 101) and decrease (e.g.,

mode 105) the HF frequencies. Remarkably, mode 245 gets shifted by approximately 150 cm^{-1} (or even more than 230 cm^{-1} if one uses a wider interpolation range and a cubic polynomial fitting). The experimentally measured peaks in solid state in KBr, as already reported by Mondal *et al.*,[8] are 3546 m, 3478 s, 3414 s, 3232w, 2924w, 1660s, 1605 s, 1584 m, 1548 m, 1474 s, 1455 s, 1383 s, 1398 m, 1384 m, 1297 m, 1228 s, 1181 s, 1108w, 1032w, 958w, 870w, 819 m, 744 m, 729 m, 685w, 637w, 584w, and 517w cm^{-1}, respectively, were w, m, and s, stand for weak, medium and strong, respectively (Figure 6). Out of those, the peaks at 584, 637, 1181 and 1297 cm^{-1} nicely match and are therefore tentatively attributed to modes 101, 105, 175 and 245 of Table 1, respectively. Mode 331 probably lies outside the experimentally measured spectrum.

3. Dynamics

The experimental investigation of the dynamics of the {Dy$_2$Ni$_2$} complex is performed with transient absorption (TA) spectroscopy. Laser pulses from the Astrella laser system (Coherent) (35 fs pulse duration, 800 nm central wavelength, 1 kHz repetition rate) were split into one part to generate the probe white light in a CaF$_2$ crystal and another part to provide the pump pulse by second harmonic generation from the fundamental (400 nm) or from the output of a non-collinear optical parametric amplifier (NOPA) (350, 320 and 300 nm). Every second pump pulse was chopped (optical chopper, AMETEK), to obtain spectra with and without pump pulse delayed via a computer controlled stage (Thorlabs). After passing the sample, the white light was refracted by a fused silica prism and recorded by a CCD Camera (Series 2000, Si Photodetector, Entwicklungsbüro Stresing). Spectra without pump pulse were subtracted from the pump-induced transient spectra which results in ΔA spectra with a time resolution < 100 fs. Data was collected and processed with in-house written Labview programs. All spectra were measured in cuvettes made of fused silica (Suprasil300, Hellma) with 1 mm optical path length at room temperature.

Time resolved spectra in a wavelength range between 350 and 700 nm were measured with an experimental setup described elsewhere.[33,70] The broad stationary absorption spectrum offers a wide pump wavelength range. Therefore, we have chosen 300, 320, 350 and 400 nm. Excitation at 300 nm leads to a spectral broad transient response between 370 and 700 nm (Figure 7, left panel). Within a few ps it converts to a band with a maximum at 480 nm tailing into the red wavelength range. The maximum shifts with time to 460 nm whereby a superposition with the ground state bleach needs to be considered between 350 and 450 nm. This leads to a negative transient response around 410 nm (no fluorescence could be found). Therefore, the apparent maxima are probably red shifted compared to the maximum of the excited state. The ground state is completely recovered within 300 ps. Excitation at longer wavelengths does not significantly change the TA spectra. A comparison is given for 460 nm probe wavelength in Figure 8. A global fit analysis with exponential decay functions reveals three processes with similar time constants for all

Figure 6. Experimental (blue line) and theoretically calculated (red line) infrared spectrum of the {Dy$_2$Ni$_2$} complex. The theoretical spectrum is at the HF level. The five vertical dashed lines indicate the frequencies which were calculated at the highly correlated CCSD level (cf. Table 1).

Table 1. Infrared frequencies (in cm^{-1}) calculated with five different methods, (analytically at the HF level, numerically at the CCSD level with a short and a longer range for the single point energy calculations, and the latter two both with a quadratic and a cubic polynomial fitting), as well as previously reported experimental results.[8] Cf. Figure 6 for the complete spectrum at the HF level.
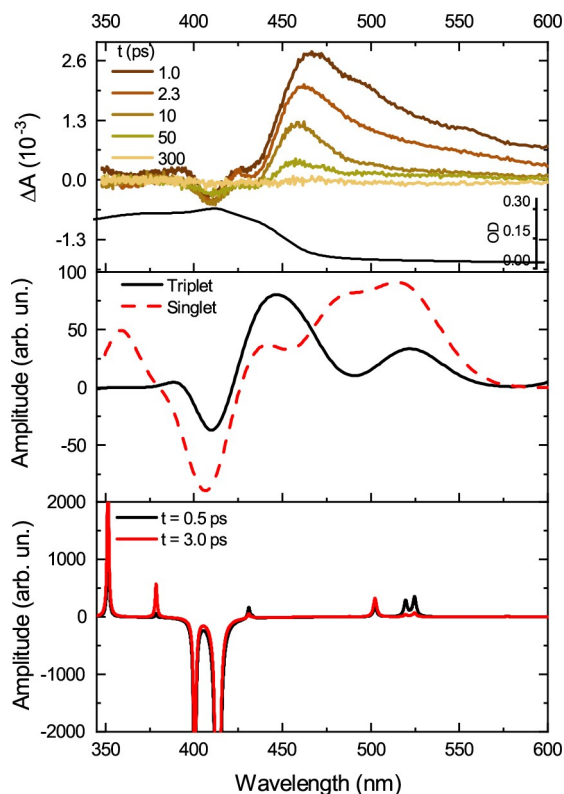
mode #	HF	wide range quadratic	cubic	short range quadratic	cubic	Exp.[8]
101	539.63	598.80	557.83	597.98	–	584
105	567.11	654.76	654.55	654.83	–	637
175	1050.42	1153.64	1544.74	1153.43	–	1181
245	1421.08	1283.23	1281.25	1282.96	1190.02	1297
331	3699.01	3706.63	3706.63	3698.49	3698.39	–

ChemistryOpen

Full Papers
doi.org/10.1002/open.202100153

Chemistry Europe
European Chemical
Societies Publishing

Figure 7. Upper panel: Experimental TA spectra at given delay times after 300 nm excitation. Absorption spectrum is shown in black for comparison. Middle panel: Theoretically calculated differential absorption spectrum, corresponding to an excitation of a 300 nm pump pulse using the WTBS $5d$ $7f$ basis set and a Gaussian broadening (standard deviation $\sigma \approx 0.38$), so that they can be directly compared with the upper panel. (Black line) for mixed populations starting from the triplet electronic states $|21\rangle - |26\rangle$, which get populated after about 1 ps. (Red dashed line), for a mixed population starting from the singlet states $|11\rangle$ and $|12\rangle$, which are populated after more than 50 ps due to electronic relaxation. Lower panel: Theoretical difference absorption spectra using the WTBS $5d$ $7f$ basis set at two different times of the propagation shown in Figure 10.
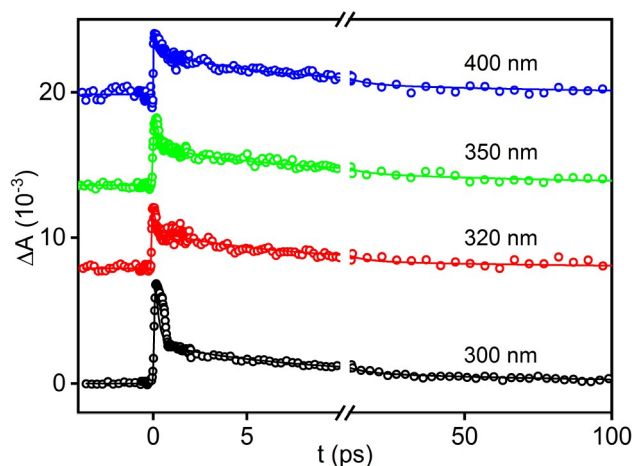
Figure 8. Comparison of experimental TA decay at 460 nm probe wavelength after 300 (black), 320 (red), 350 (green) and 400 (blue) nm excitation. Circles: measured data points, lines: fit functions. ΔA values were referenced at 2 ps for better comparison.

excitation wavelengths. The amplitudes for the exponential decay functions received from global analysis exemplarily for 300 and 400 nm excitation are given in decay associated spectra (DAS) in Figure 9.

A first time constant was obtained within few hundred fs (τ_1) after 400 nm photoexcitation, which for the 300 nm excitation is masked by artifacts (mainly chirp and group velocity mismatch). A second time constant on the ps range (τ_2) is somewhat larger for 400 nm excitation than for 300 nm. The longest time constant was found to be around 70 ps (τ_3) (Table 2). No longer-lived components were observed indicating that the system relaxes back to the ground state indicating no significant photo instabilities. It is known for α-Fe$_2$O$_3$ nanoparticles[71] and for α-Fe$_2$O$_3$ thin films[72] that after O^{-2} $2p$ excitation into the conduction band vibrational relaxation as well as trapping into $d-d$ states from the Fe occurs on a hundred fs timescale. Subsequent geminal recombination can be observed within few ps whereas the trapped electrons live some tens of ps. In case of NiO thin films, the relaxation dynamics is similar but with an additional long lived (several ns) trap state exists.[34] The three step relaxation process can also be
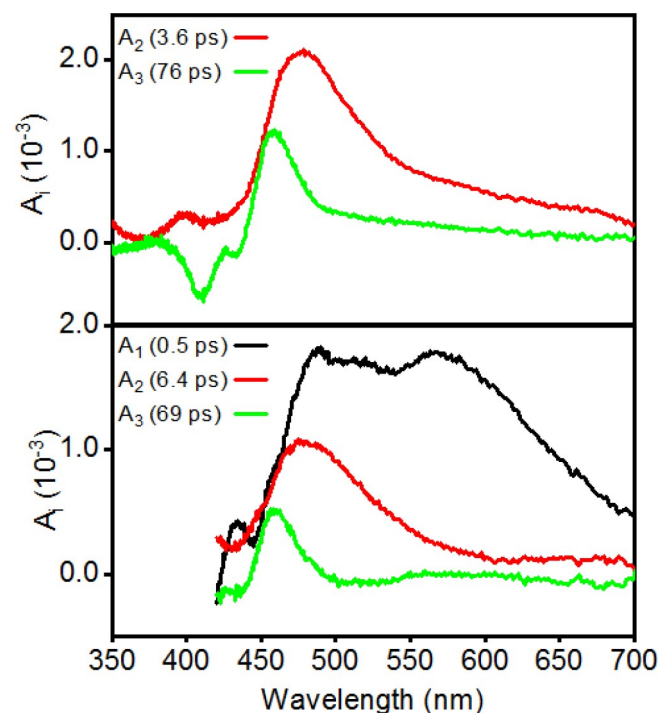
Figure 9. Experimental decay associated spectra obtained from global analysis for 300 nm excitation (upper panel) and 400 nm excitation (lower panel). Evaluation of the first time constant is not possible after 300 nm excitation due to artifacts on that time scale. Scattering from the pump pulse after 400 nm excitation hinders analysis in this region.

Table 2. Experimentally derived time constants from global analysis after 300 and 400 nm excitation.

	300 nm	400 nm
τ_1 (ps)	–	0.5
τ_2 (ps)	3.6	6.4
τ_3 (ps)	76	69

ChemistryOpen

Full Papers
doi.org/10.1002/open.202100153

Chemistry
Europe
European Chemical
Societies Publishing

found for $Fe_{10}Ln_{10}$ clusters.[3] Considering the relatively close structural absorptive properties, an analogue interpretation is given here. Consequently, we attribute the first time constant τ_1 after photoexcitation of the O–Ni unit to vibrational relaxation and trapping processes, τ_2 to geminal recombination, and τ_3 to the lifetime of the trap states. In molecular systems, the optical transitions are usually dictated by electrons which are close to the Fermi level (i.e., near the HOMO) and contribute substantially to the correlations through virtual excitations (in other words they move "more freely" than the deeper lying stronger "bound" core electrons). Our system, containing two $3d$ and two $4f$ interacting magnetic atoms although not (quasi-)infinitely extended like nanoparticles, it still possesses states of different multiplicities which are inert enough, so that spin-crossover transitions become slower than in other mono-metallic systems, such as $Cr(acac)_3$[73] or Fe(II) complexes.[74–78]

In general, the very-early-time dynamics requires calculations under non-equilibrium conditions and reflects the intra-molecular vibrational redistribution (IVR), which takes place after the initial Franck-Condon excitation. This, although very interesting, goes well beyond the scope of this work, which focuses on the electronic dynamics. Furthermore, the wavelength dependence of the IVR is still a challenging task (under debate in many systems and often not known). Here, solid state measurements or better solvents could give access to the earliest events like vibrational relaxation and trapping. This technique, however, would remain to future studies and is currently not available. The system does not relax to the ground state distribution (Boltzmann distribution) on the electronic time scale (τ_2). Only on longer time scales (τ_3), when the phononic contributions become significant, a complete thermalization occurs.

As a first attempt to theoretically explain the observed behavior we look at the differential absorption spectra of the excited states, which are most probably populated by the 300 nm (4.13 eV) pump pulse. For both basis sets we find the substates of two triplet states at this energy region. Here, we exemplarily mention the WTBS results, namely two triplet states from $|21\rangle$ to $|26\rangle$, with energies from 2.37 eV (523 nm) up to 2.83 eV (438 nm) with very similar electronic absorption spectra. Thus the most pronounced peak at 2.68 eV (462 nm) which is experimentally observed after about 1 ps (Figure 7, left panel), corresponds to excitations from states $|21\rangle - |26\rangle$ to states $|95\rangle$ at 6.61 eV (188 nm), $|98\rangle$ at 6.62 eV (187 nm), $|102\rangle$ at 6.91 eV (179 nm), $|107\rangle$ at 7.02 eV (177 nm), and $|110\rangle$ at 7.07 eV (175 nm), as shown by the black line in Figure 7. The dip at 3.03 eV (409 nm) which appears at the same time, is due to the depopulation of the ground state. The peak corresponds almost perfectly to the excitation from the ground state to state $|8\rangle$ with energy 3.04 eV (408 nm). The red dashed line of Figure 7 corresponds to a possible short-lived combination of the quasi degenerate singlet states $|11\rangle$ and $|12\rangle$, with energy 3.16 eV (392 nm). These are our lowest calculated singlet states, which in time-resolved experiments can only appear at much later times since the electronic relaxation towards them is spin-forbidden. We also find a theoretical peak at about 550 nm

which, however, could not be observed in our experimental data, possibly due to a very weak oscillator strength.

For a more exact description we theoretically propagate the system's density matrix

$$\hat{\rho}(t) = -i\big[\hat{H}(t), \hat{\rho}(t)\big] + L[\rho(t)], \qquad (1)$$

where $\hat{H}(t)$ is the system's time-dependent Hamiltonian (including the laser pulses used in the experimental setup) and $[.,.]$ is the commutator operator. $L[.]$ is the Lindblad superoperator
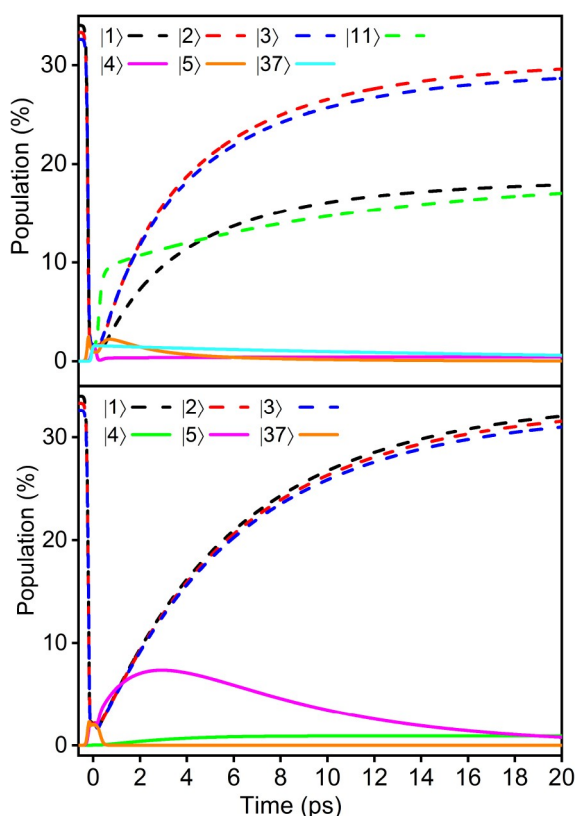
$$L[\rho(t)] = \kappa \sum_j \gamma_j \left(\hat{A}_j \hat{\rho}(t) \hat{A}_j^\dagger - \frac{1}{2} \left\{ \hat{A}_j^\dagger(\omega) \hat{A}_j, \hat{\rho}_S \right\} \right), \qquad (2)$$

and describes the interaction with the thermal bath (leading to relaxation and decoherence). $\{.,.\}$ is the anticommutator operator. Each temperature-dependent parameter γ_j is pertinent to the j-th bath-induced transition, and is described by a pair of creator and annihilator operators A_j and $A_j^\dagger$. κ is an overall system-bath coupling constant. Physically the coupling, the nature of which is not explicitly described with this formalism, can occur due to exchange of photons, phonons or even electrons between the system and the bath (or any combination of those). We restrict the bath-induced transitions to the dipole allowed transitions and weigh them accordingly (since the energy exchange between the system and the bath mainly occurs through electrostatic interactions; additional channels, e.g., phonons, do not change the selection rules but merely strengthen this interaction; this can be taken into account by adjusting the coupling constants κ or γ_i). As seen in Eq. (1) we simultaneously propagate under the influence of both the optical perturbation and the heat exchange.

Figure 10 shows some selected time-dependent state populations for the two basis sets, and a pump laser pulse of 300 nm. In both cases the lowest three states, which stem from the same triplet, get depopulated during the pulse and repopulated during the relaxation. An interesting detail is that some states are clearly populated through relaxation only, since they reach their maximum population after the laser pulse (for example state $|5\rangle$ for the SARC-ZORA basis set reaches the maximum population after about 2 ps). Since these intermediate states strongly contribute to the thermal non-equilibrium of the system [see Eq. (3) further below], their population and depopulation speeds dictate the relaxation times.

Let us look a bit closer to the dynamics the system calculated with the SARC-ZORA basis set (Figure 10 upper panel), which has a special characteristic, namely the trap state $|11\rangle$ in the low-energy tail, not found with the WTBS basis set. State $|11\rangle$ stems mainly from a singlet state and has allowed electric-dipole transition only to energetically higher electronic states, therefore its population relaxes only extremely slowly back to the triplet ground state (through additional channels, e.g., phonons). The main virtual transitions which contribute to the trap state $|11\rangle$ are $341/342 \rightarrow 346$ with amplitudes 0.289 and 0.200, respectively (Figure 3). In general we expect a

ChemistryOpen

Full Papers
doi.org/10.1002/open.202100153

Chemistry Europe
European Chemical
Societies Publishing

Figure 10. Theoretical propagation of the 300 nm probe pulse on the {Dy$_2$Ni$_2$} complex calculated with the SARC-ZORA (upper) and the WTBS (lower) basis sets. In both cases the system is coupled to a bath of $T = 300$ K with a coupling strength of $\kappa = 3.0 \times 10^{-5}$ (cf. Table 3). The solid and the dashed lines refer to states with very low and appreciable population at the end of our propagation (20 ps), respectively.

Boltzmann distribution at $t \rightarrow \infty$. However, for time scales at which one can neglect electron-phonon coupling the system does not relax to a thermalized distribution. This trapping effect can also be seen in the experimental data (cf. Figures 7 and 8).

Since a similar trapping state is not found with the WTBS basis set we do not find a significant difference in the propagation of $\sigma(t)$ [cf. Eq. (3) for the two different pump pulses (300 and 400 nm)]. In both propagations an inspection of the electronic overlap distribution and the virtual transitions between the metal and the oxygen atoms for the different participating states (not shown here), unveils the significance of the charge-transfer contributions for the coupling to the laser pulse. However, due to the heavily correlated character of the many-body electronic states, as well as the classical and quantum superpositions of numerous states, a simple Mulliken population analysis (which relies on the lossy reduction of the full density matrix to the one-electron density matrix) only shows rather small charge redistributions (of the order of 0.3 and 0.2 for Dy and Ni, respectively).

The theoretical relaxation times (Table 3) are computed with a Fourier transform of the time-dependent standard deviation of the populations from the Boltzmann distribution for a given temperature T

$$\sigma(t) = \sqrt{\sum_{i=1}^{n}[p_i^{\text{Boltz.}} - p_i(t)]^2}, \qquad (3)$$

where n is the number of states, while $p_i^{\text{Boltz.}}$ and $p_i(t)$ are the thermal-equilibrium (Boltzmann distribution) population and the actual calculated time-dependent population of state $|i\rangle$, respectively.

In relation to the ground state spectra (cf. Figure 5) we can extract the TA difference spectra for different times t from the population propagation. The theoretical TA spectra for $t = 0.5$ and 3.0 ps are shown in Figure 7 (right panel). The ground state spectrum for 300 K is already subtracted, which is the reason for the negative values. The two small peaks between 500 and 550 nm as well as the even smaller peak below 450 nm decrease for increasing delay t. For the positive peaks at 500 nm and between 350 and 400 nm it is the opposite.

Table 3. Theoretically calculated electronic relaxation times τ_2 on the ligand stabilized {Dy$_2$Ni$_2$} complex calculated with the CCSD method and the WTBS basis set and excited with both pulses, 400 and 300 nm and different coupling constants κ_2. The relaxation times have been extracted from a Fourier transform.

	SARC-ZORA		WTBS	
κ ($\times 10^{-5}$)	400 nm τ_2 (ps)	300 nm τ_2 (ps)	400 nm τ_2 (ps)	300 nm τ_2 (ps)
1	6.57	7.05	42.43	13.62
2	3.27	3.38	13.62	6.73
3	2.22	2.26	6.69	4.43
4	1.70	1.72	4.41	3.29
5	1.36	1.39	3.27	2.61
6	1.15	1.17	2.60	2.16
7	0.99	1.01	2.15	1.84
8	0.88	0.89	1.83	1.60
9	0.79	0.79	1.40	1.42
10	0.69	0.70	1.26	1.27
20	0.37	0.38	0.60	0.61
30	0.26	0.28	0.39	0.40
40	0.22	0.20	0.29	0.29
50	0.16	0.16	0.23	0.23

ChemistryOpen

Full Papers
doi.org/10.1002/open.202100153

Chemistry Europe
European Chemical
Societies Publishing

For WTBS all τ_2 are larger, especially for the pump pulse with larger wavelength, while it is the other way around for SARC-ZORA (Table 2). The differences between them can be attributed to the additional trap state $|11\rangle$ of the SARC-ZORA basis set, which is not found with the WTBS basis set, and exhibits the strongest transition channels to very high lying states (above 6 eV), while transitions to the states $|16\rangle$, $|17\rangle$, and $|36\rangle$ are extremely weak. In contrast the transitions to the ground state originate mostly from states between $|24\rangle$ and $|57\rangle$. As a result, the stronger the overall excitation of the system (i.e., more intense laser pulse), the more population is ultimately driven to trap state $|11\rangle$ in lieu of the ground state, thus delaying the relaxation to a thermalized (Boltzmann) distribution. A comparison between experimental and theoretical τ_2 values makes us roughly estimate a κ value between 1×10^{-5} and 2×10^{-5} for the SARC-ZORA and between 3×10^{-5} and 4×10^{-5} for the WTBS basis sets.

Due to the finite time scale of the theoretical propagation and the fact, that slower relaxation channels (e.g., phonons) are only indirectly taken into account through the coupling constants κ and γ_i, it is not possible to explicitly calculate τ_3. However, there is a nice qualitative similarity between the theoretical differential absorption spectra of the singlet states $|11\rangle$ and $|12\rangle$ (red dashed line of the center panel of Figure 7) and the experimental decay associated spectrum for 300 nm pulse excitation (green line in the upper panel of Figure 9), which strongly suggests that at least the experimentally observed relaxation time $\tau_3 = 76$ ps is due to the slow, spin-forbidden transitions $|11\rangle \rightarrow |1\rangle$ and $|12\rangle \rightarrow |1\rangle$. This is more than 15 times longer than the lifetime of the analogous trapping state found in the $\left[Ni_2^{II}(\mathbf{L}-\mathbf{N}_4Me_2)(emb)\right]$ complex,[35] and we ascribe this difference to the presence of the Dy atoms.

4. Summary

In this joint theoretical and experimental study we look into the details of photoexcitation of a Dy_2Ni_2 compound. Our main results are: (i) By comparing the experimental and the theoretical electronic absorption spectra of the compound, we do not only establish the quality of the theoretical calculations needed for an appropriate description of the dynamics, but also qualitatively identify the correlation contributions to the laser excitations, as well as the pertinent charge-transfer virtual excitations. Generally, the SARC-ZORA results describe better the long wavelength region (low-energy tail) of the statinary spectra, whereas the WTBS results agree better with the femtosecond/picosecond experimentally observed dynamics. (ii) We experimentally excite our compound with four different pump pulses (300, 320, 350, and 400 nm), and extract two relaxation times for the the 300 nm pulse, and three relaxation times for the 400 nm pulse. (iii) We theoretically propagate the total electronic many-body wavefunction of the system with the same laser pulses, and we can thus explain the behavior of the experimentally observed results. More specifically, we (iv) identify the intermediate states of the laser excitation (by comparing their absorption spectra with the experimental

ones), (v) unveil the (partial) metal-to-oxygen charge transfer excitations in the dynamics (by inspecting the molecular orbitals contributing to the pertinent many-body states), (vi) estimate the system-to-bath coupling constant κ, and (vii) detect a trapping intermediate state which explicitly explains the slowest relaxation time. Our successful ansatz and our findings give insight into the microscopic mechanisms of the experimentally observed dynamics of this prototypic single molecule magnet compound, thus facilitating a more targeted design of other compounds with similar but slightly different dynamics properties.

Conflict of Interest

The authors declare no conflict of interest.

Data Availability Statement

The data that support the findings of this study are available from the corresponding author upon reasonable request.

[1] K. C. Mondal, A. Sundt, Y. Lan, G. E. Kostakis, O. Waldmann, L. Ungur, L. F. Chibotaru, C. E. Anson, A. K. Powell, *Angew. Chem.* **2012**, *51*, 7550.

[2] Y. Peng, V. Mereacre, C. E. Anson, A. K. Powell, *Dalton Trans.* **2017**, *46*, 5337.

[3] A. Baniodeh, Y. Liang, C. E. Anson, N. Magnani, A. K. Powell, A.-N. Unterreiner, S. Seyfferle, M. Slota, M. Dressel, L. Bogani, K. Goß, *Adv. Funct. Mater.* **2014**, *24*, 6280.

[4] K. Griffiths, I. A. Kühne, G. J. Tizzard, S. J. Coles, G. E. Kostakis, A. K. Powell, *Inorg. Chem.* **2019**, *58*, 2483.

[5] W. Wernsdorfer, M. Ruben, *Adv. Mater.* **2019**, *31*, 1806687.

[6] D. Shao, X.-Y. Wang, *Chin. J. Chem.* **2020**, *38*, 1005.

[7] D. N. Woodruff, R. E. P. Winpenny, R. A. Layfield, *Chem. Rev.* **2013**, *113*, 5110.

[8] K. C. Mondal, G. E. Kostakis, Y. L. W. Wernsdorfer, C. E. Anson, A. K. Powell, *Inorg. Chem.* **2011**, *50*, 11604.

[9] J. Wu, L. Zhao, P. Zhang, L. Zhang, M. Guo, J. Tang, *Dalton Trans.* **2015**, *44*, 11935.

[10] M. Andruh, J.-P. Costes, C. Diaz, S. Gao, *Inorg. Chem.* **2009**, *48*, 3342.

[11] J.-C. G. Bünzli, *J. Coord. Chem.* **2014**, *67*, 3706.

[12] Z. Zheng, *Recent development in clusters of rare earths and actinides: Chemistry and materials*, Structure and bonding, Springer, Berlin, Heidelberg, **2016**, pp. 339.

[13] N. Pooransingh, E. Pomerantseva, M. Ebel, S. Jantzen, D. Rehder, T. Polenova, *Inorg. Chem.* **2003**, *42*, 1256.

[14] A. M. Ako, V. Mereacre, I. J. Hewitt, R. Clérac, L. Lecren, C. E. Anson, A. K. Powell, *J. Mater. Chem.* **2006**, *16*, 2579.

[15] A. Mishra, W. Wernsdorfer, S. Parsons, G. Christou, E. K. Brechin, *Chem. Commun.* **2005**, *16*, 2086.

[16] M. Murugesu, A. Mishra, W. Wernsdorfer, K. A. Abboud, G. Christou, *Polyhedron* **2006**, *25*, 613.

[17] J. Rinck, G. Novitchi, W. V. d. Heuvel, L. Ungur, Y. Lan, W. Wernsdorfer, C. E. Anson, L. F. Chibotaru, A. K. Powell, *Angew. Chem. Int. Ed.* **2010**, *49*, 7583.

[18] V. Mereacre, A. M. Ako, R. Clérac, W. Wernsdorfer, I. J. Hewitt, C. E. Anson, A. K. Powell, *Chem. Eur. J.* **2008**, *14*, 3577.

[19] V. Mereacre, Y. Lan, R. Clerac, A. M. Ako, I. J. Hewitt, W. Wernsdorfer, G. Buth, C. E. Anson, A. K. Powell, *Inorg. Chem.* **2010**, *49*, 5293.

ChemistryOpen

Full Papers
doi.org/10.1002/open.202100153

Chemistry Europe
European Chemical
Societies Publishing

[20] D. Schray, G. Abbas, Y. Lan, V. Mereacre, A. Sundt, J. Dreiser, O. Waldmann, G. E. Kostakis, C. E. Anson, A. K. Powell, *Angew. Chem. Int. Ed.* **2010**, *49*, 5185.

[21] V. Chandrasekhar, B. M. Pandian, R. Azhakar, J. J. Vittal, R. Clérac, *Inorg. Chem.* **2007**, *46*, 5140.

[22] E. Pointillart, K. Bernot, R. Sessoli, D. Gatteschi, *Chem. Eur. J.* **2007**, *13*, 1602.

[23] V. Chandrasekhar, B. M. Pandian, R. Boomishankar, A. Steiner, J. J. Vittal, A. Houri, R. Clérac, *Inorg. Chem.* **2008**, *47*, 4918.

[24] J.-P. Sutter, S. Dhers, R. Rajamani, S. Ramasesha, J.-P. Costes, C. Duhayon, L. Vendier, *Inorg. Chem.* **2009**, *48*, 5820.

[25] C. G. Efthymiou, T. C. Stamatatos, C. Papatriantafyllopoulou, A. J. Tasiopoulos, W. Wernsdorfer, S. P. Perlepes, G. Christou, *Inorg. Chem.* **2009**, *48*, 9737.

[26] T. Yamaguchi, J.-P. Costes, Y. Kishima, M. Kojima, Y. Sunatsuki, N. Bréfuel, J.-P. Tuchagues, L. Vendier, W. Wernsdorfer, *Inorg. Chem.* **2010**, *49*, 9125.

[27] T. D. Pasatoiu, M. Etienne, A. M. Madalan, M. Andruh, R. Sessoli, *Dalton Trans.* **2010**, *39*, 4802.

[28] Y. Gao, L. Zhao, X. Xu, G.-F. Xu, Y.-N. Guo, J. Tang, Z. Liu, *Inorg. Chem.* **2011**, *50*, 1304.

[29] T. D. Pasatoiu, J.-P. Sutter, A. M. Madalan, F. Z. C. Fellah, C. Duhayon, M. Andruh, *Inorg. Chem.* **2011**, *50*, 5890.

[30] E. Colacio, J. Ruiz-Sanchez, F. J. White, E. K. Brechin, *Inorg. Chem.* **2011**, *50*, 7268.

[31] G. Novitchi, W. Wernsdorfer, L. F. Chibotaru, J.-P. Costes, C. E. Anson, A. K. Powell, *Angew. Chem. Int. Ed.* **2009**, *48*, 1614.

[32] R. Berera, R. van Grondelle, J. T. M. Kennis, *Photosynth. Res.* **2009**, *101*, 105.

[33] N. C. Michenfelder, C. Gienger, A. Schnepf, A.-N. Unterreiner, *Dalton Trans.* **2019**, *48*, 15577.

[34] L. D'Amario, J. Föhlinger, G. Boschloo, L. Hammarström, *Chem. Sci.* **2018**, *9*, 223.

[35] W. Jin, F. Rupp, K. Chevalier, M. M. N. Wolf, M. C. Rojas, G. Lefkidis, H.-J. Krüger, R. Diller, W. Hübner, *Phys. Rev. Lett.* **2012**, *109*, 267209.

[36] H.-P. Breuer, F. Petruccione, *The theory of open quantum systems*, Oxford University Press, Oxford, **2002**, pp. 620.

[37] E. Beaurepaire, J.-C. Merle, A. Daunois, J.-Y. Bigot, *Phys. Rev. Lett.* **1996**, *76*, 4250.

[38] J. Hohlfeld, E. Matthias, R. Knorren, K. H. Bennemann, *Phys. Rev. Lett.* **1997**, *78*, 4861.

[39] A. Scholl, L. Baumgarten, R. Jacquemin, W. Eberhardt, *Phys. Rev. Lett.* **1997**, *79*, 5146.

[40] M. Aeschlimann, M. Bauer, S. Pawlik, W. Weber, R. Burgermeister, D. Oberli, H. C. Siegmann, *Phys. Rev. Lett.* **1997**, *79*, 5158.

[41] C. Stamm, T. Kachel, N. Pontius, R. Mitzner, T. Quast, K. Holldack, S. Khan, C. Lupulescu, E. F. Aziz, M. Wietstruk, H. A. Dürr, W. Eberhardt, *Nat. Mater.* **2007**, *6*, 740.

[42] C. Boeglin, E. Beaurepaire, V. Halté, V. López-Flores, C. Stamm, N. Pontius, H. A. Dürr, J.-Y. Bigot, *Nature* **2010**, *465*, 458.

[43] F. Liedy, R. Shi, M. Coletta, J. Vallejo, E. K. Brechin, G. Lefkidis, W. Hübner, J. O. Johansson, *J. Magn. Magn. Mater.* **2020**, *501*, 166476.

[44] R. Gómez-Abal, O. Ney, K. Satitkovitchai, W. Hübner, *Phys. Rev. Lett.* **2004**, *92*, 227402.

[45] R. Gómez-Abal, W. Hübner, *Phys. Rev. B* **2002**, *65*, 195114.

[46] W. Hübner, G. P. Zhang, *Phys. Rev. B* **1998**, *58*, R5920.

[47] H. Xiang, G. Lefkidis, W. Hübner, *Phys. Rev. B* **2012**, *86*, 134402.

[48] G. P. Zhang, W. Hübner, *Phys. Rev. Lett.* **2000**, *85*, 3025.

[49] D. Chaudhuri, G. Lefkidis, W. Hübner, *Phys. Rev. B* **2017**, *96*, 184413.

[50] C. Li, S. Zhang, W. Jin, G. Lefkidis, W. Hübner, *Phys. Rev. B* **2014**, *89*, 184404.

[51] G. Lefkidis, W. Jin, J. Liu, D. Dutta, W. Hübner, *J. Phys. Chem. Lett.* **2020**, *11*, 2592.

[52] D. Chaudhuri, H. P. Xiang, G. Lefkidis, W. Hübner, *Phys. Rev. B* **2014**, *90*, 245113.

[53] S. Sold, G. Lefkidis, B. Kamble, J. Berakdar, W. Hübner, *Phys. Rev. B* **2018**, *97*, 184428.

[54] T. Ferté, N. Bergeard, L. Le Guyader, M. Hehn, G. Malinowski, E. Terrier, E. Otero, K. Holldack, N. Pontius, C. Boeglin, *Phys. Rev. B* **2017**, *96*, 134303.

[55] D. Dutta, G. Lefkidis, W. Hübner, *Phys. Scr.* **2020**, *95*, 065805.

[56] P. R. Taylor, *Coupled-cluster Methods in Quantum Chemistry*, 64, Springer, Berlin, Heidelberg, **1994**, 344 pp.

[57] S. K. Mukhopadhyay, R. Chaudhuri, D. Mukhopadhyay, D. Mukherjee, *Chem. Phys. Lett.* **1990**, *173*, 181.

[58] A. I. Krylov, *Annu. Rev. Phys. Chem.* **2008**, *59*, 433.

[59] G. D. Purvis III, R. J. Bartlett, *J. Chem. Phys.* **1982**, *76*, 1910.

[60] J. Cizek, *J. Chem. Phys.* **1966**, *45*, 4256.

[61] R. J. Bartlett, *J. Phys. Chem.* **1989**, *93*, 1697.

[62] K. Kowalski, P. Piecuch, *J. Chem. Phys.* **2004**, *120*, 1715.

[63] M. W. Schmidt, K. K. Baldridge, J. A. Boatz, S. T. Elbert, M. S. Gordon, J. H. Jensen, S. Koseki, N. Matsunaga, K. A. Nguyen, S. Su, T. L. Windus, M. Dupuis, J. A. Montgomery, *J. Comput. Chem.* **1993**, *14*, 1347.

[64] W. J. Hehre, R. F. Stewart, J. A. Pople, *J. Chem. Phys.* **1969**, *51*, 2657.

[65] T. Noro, M. Sekiya, T. Koga, *Theor. Chem. Acc.* **2012**, *131*, 1124.

[66] D. A. Pantazis, F. Neese, *J. Chem. Theory Comput.* **2009**, *5*, 2229.

[67] S. Huzinaga, B. Miguel, *Chem. Phys. Lett.* **1990**, *175*, 289.

[68] S. Huzinaga, M. Klobukowski, *Chem. Phys. Lett.* **1993**, *212*, 260 .

[69] D. Dutta, M. Becherer, D. Bellaire, F. Dietrich, M. Gerhards, G. Lefkidis, W. Hübner, *Phys. Rev. B* **2018**, *97*, 224404.

[70] C. Schweigert, O. Babii, S. Afonin, T. Schober, J. Leier, N. C. Michenfelder, I. V. Komarov, A. S. Ulrich, A. N. Unterreiner, *ChemPhotoChem* **2019**, *3*, 403.

[71] S. Baskoutas, A. F. Terzis, *J. Appl. Phys.* **2006**, *99*, 013708.

[72] A. G. Joly, J. R. Williams, S. A. Chambers, G. Xiong, W. P. Hess, D. M. Laman, *J. Appl. Phys.* **2006**, *99*, 053521.

[73] E. A. Juban, J. K. McCusker, *J. Am. Chem. Soc.* **2005**, *127*, 6857.

[74] M. C. Carey, S. L. Adelman, J. K. McCusker, *Chem. Sci.* **2019**, *10*, 134.

[75] P. Chábera, K. S. Kjaer, O. Prakash, A. Honarfar, Y. Liu, L. A. Fredin, T. C. B. Harlang, S. Lidin, J. Uhlig, V. Sundström, R. Lomoth, P. Persson, K. Wärnmark, *J. Phys. Chem. Lett.* **2018**, *9*, 459.

[76] J. Steube, L. Burkhardt, A. Päpcke, J. Moll, P. Zimmer, R. Schoch, C. Wölper, K. Heinze, S. Lochbrunner, M. Bauer, *Chem. Eur. J.* **2019**, *25*, 11826.

[77] Y. Liu, K. S. Kjær, L. A. Fredin, P. Chábera, T. Harlang, S. E. Canton, S. Lidin, J. Zhang, R. Lomoth, K.-E. Bergquist, P. Persson, K. Wärnmark, V. Sundström, *Chem. Eur. J.* **2015**, *21*, 3628.

[78] P. Zimmer, L. Burkhardt, A. Friedrich, J. Steube, A. Neuba, R. Schepper, P. Müller, U. Flörke, M. Huber, S. Lochbrunner, M. Bauer, *Inorg. Chem.* **2018**, *57*, 360.